

# Parameterized Molecular Cavity Quantum Electrodynamics Approach to Simulate van der Waals Interactions<sup>†</sup>

Sebastian Montillo Vega,<sup>‡</sup> Sanchari Sannigrahi,<sup>‡</sup> Braden M. Weight,<sup>\*,¶</sup> and Pengfei Huo<sup>\*,‡,§,||</sup>

<sup>‡</sup>*Department of Chemistry, University of Rochester, Rochester, NY 14627, U.S.A.*

<sup>¶</sup>*Theoretical Division, Los Alamos National Laboratory, Los Alamos, NM 87545, U.S.A.*

<sup>§</sup>*The Institute of Optics, Hajim School of Engineering, University of Rochester, Rochester, NY 14627, U.S.A.*

<sup>||</sup>*Center for Coherence and Quantum Optics, University of Rochester, Rochester, New York 14627, U.S.A.*

E-mail: braden.m.weight@lanl.gov; pengfei.huo@rochester.edu

## Abstract

The strong coupling between light and matter inside optical cavities has emerged as a strategy to modify the chemical and physical properties of materials. In this work, we explore the performance of the recently developed parameterized quantum electrodynamics (pQED) approach based on time-dependent density functional theory (TDDFT) for non-covalently interacting systems, including van der Waals and hydrogen bonding interactions. We find that the pQED-TDDFT approach accurately reproduces the cavity-modified potential energy surfaces of the polaritonic ground state, compared with high-level QED coupled-cluster and state-of-the-art QED density functional theory results. By computing the ground-state density difference, we show that the dispersion-energy modifications are due to electronic density redistribution inside the cavity. We further explore the convergence properties of the pQED-TDDFT method as functions of the number of electronic states  $N_{\text{el}}$  and the number of photonic Fock states  $N_{\text{F}}$ . We find reliable, but highly fluctuating, convergence of the ground state energy as a function of the number of electronic states  $N_{\text{el}} \sim 10^2 - 10^4$  yet quickly and monotonically convergent in the number of Fock states  $N_{\text{F}} \leq 2$ . This work establishes the scope and limitations of current *ab initio* treatments of cavity-modified dispersion forces and provides a foundation for developing predictive theoretical tools in polaritonic chemistry.

## Introduction

The strong coupling between light and matter inside optical cavities has emerged as a strategy to modify chemical and physical properties of materials.<sup>1–4</sup> By hybridizing molecular excitations with confined photon modes, new quasiparticles – so called polaritons – arise that can alter photochemical reactivity,<sup>5–8</sup> energy/charge transfer,<sup>9–11</sup> as well as ground-state energetics.<sup>12–15</sup> While many experimental works have shown such effects in the excited state, however sometimes lacking solid theoretical understanding of the modified chemical or physical mechanisms, polaritonic effects on weak intermolecular interactions such as hydrogen bonding and dispersion forces remains poorly explored and not well understood from both theoretical and experimental perspectives.<sup>16–18</sup>

Many of the theoretical challenges presented by polaritonic chemistry relate either to the collective nature of the problem, where many molecules can simultaneously couple to many cavity modes, or to the treatment of *ab initio* many-body correlations. In this work, we focus on the treatment of the many-body correlations, acknowledging that collective effects may be equally important. For the single-molecule and single-cavity-mode case, the most commonly used model for describing a polaritonic system is the Pauli-Fierz Hamiltonian in the Born-Oppenheimer, dipole, and

<sup>†</sup>LA-UR-25-31319

long-wavelength approximations

$$\hat{H}_{\text{PF}}(\mathbf{R}) = \hat{H}_{\text{el}}(\mathbf{R}) + \hat{H}_{\text{ph}} + \frac{\lambda^2}{2}(\hat{\mu}(\mathbf{R}) \cdot \hat{e})^2 + \sqrt{\frac{\omega_c}{2}}\lambda(\hat{\mu}(\mathbf{R}) \cdot \hat{e})(\hat{a}^\dagger + \hat{a}). \quad (1)$$

Here,  $\hat{H}_{\text{el}} = \hat{T}_e + \hat{V}_{eN}(\mathbf{R}) + \hat{V}_{ee} + V_{NN}(\mathbf{R})$  is the standard electronic Hamiltonian,  $\hat{H}_{\text{ph}} = \hbar\omega_c \hat{a}^\dagger \hat{a}$  is the photonic Hamiltonian,  $\hat{H}_{\text{el-ph}}(\mathbf{R}) = \sqrt{\frac{\omega_c}{2}}\lambda(\hat{\mu}(\mathbf{R}) \cdot \hat{e})(\hat{a}^\dagger + \hat{a})$  is the light-matter interaction, and  $\hat{H}_{\text{DSE}}(\mathbf{R}) = \frac{\lambda^2}{2}(\hat{\mu}(\mathbf{R}) \cdot \hat{e})^2$  is the dipole self-energy. The light-matter coupling strength is defined as,

$$\lambda = \sqrt{\frac{1}{\varepsilon_0 \mathcal{V}}} \hat{e} = \sqrt{2\omega_c} \mathbf{A}_0, \quad (2)$$

where  $\varepsilon_0$  is the electric permittivity,  $\mathcal{V}$  is the cavity mode volume, and  $\hat{e}$  is the cavity polarization.

Two approaches exist to model the polaritonic problem. The first allows for a self-consistent (sc) solution by directly extending standard many-body approaches, such as quantum electrodynamic Hartree-Fock (scQED-HF),<sup>14</sup> density functional theory (scQED-DFT),<sup>19,20</sup> coupled cluster theory (scQED-CC),<sup>14,21</sup> complete active space (scQED-CAS),<sup>22</sup> configuration interaction (scQED-CI),<sup>21,23</sup> quantum Monte Carlo (scQED-QMC),<sup>24,25</sup> and many others. We refer to these approaches as *ab initio* self-consistent quantum electrodynamics (scQED-X) approaches.

The second approach is to use the output from standard quantum chemical software, which solves the complicated electronic Hamiltonian  $\hat{H}_{\text{el}}(\mathbf{R})$  at an appropriate level of theory for the molecular system. Following this, polaritonic Hamiltonian is constructed in the product basis of the adiabatic electronic states  $|\psi_\alpha(\mathbf{R})\rangle$  (eigenstates of  $\hat{H}_{\text{el}}(\mathbf{R})$ ) and the Fock states (or number states) of the cavity mode  $|n\rangle$  (eigenstates of  $\hat{H}_{\text{ph}}$ ). Since the polaritonic Hamiltonian is parameterized by the adiabatic electronic information, we denote this approach as parameterized QED (pQED),<sup>15,26</sup> which can be combined with any electronic structure approach.

The difficulty of accurately solving the polaritonic problem arises when trying to simultaneously treat electron-electron, photon-mediated electron-electron, and electron-photon correlations. In the scQED approach, these correlations are necessarily treated at the same level, regardless of the many-body approach used. For example, extensions such as scQED-DFT provide a formally ex-

act framework, but its accuracy depends on the design of exchange-correlation functionals that account for all of the above-mentioned multi-body correlations. Further, as recently explored in Ref. 27, the anisotropy, the direction-dependent nature of electron-photon interactions determined by the relative orientation of the molecular dipole with respect to the cavity polarization  $\hat{\mu} \cdot \hat{e}$ , and higher-order electron-photon processes, provides a unique challenge in designing modern exchange-correlation functionals which encapsulate these effects. More specifically, Ref. 27 introduced the photon many-body dispersion (pMBD) method as a density-based approach that extends fluctuation-dissipation theory to electron-photon systems, offering a promising route to describe cavity-modified dispersion interactions with modest computational effort.

In the pQED framework, the electron-photon and photon-mediated electron-electron interactions are treated exactly through direct diagonalization of the light-matter Hamiltonian to yield polaritonic eigenstates  $|\Phi_j(\mathbf{R})\rangle$  and potential energy surfaces  $E_j(\mathbf{R})$

$$\hat{H}_{\text{PF}} |\Phi_j(\mathbf{R})\rangle = E_j(\mathbf{R}) |\Phi_j(\mathbf{R})\rangle, \quad (3)$$

where the polaritonic eigenstates are expanded in the adiabatic-Fock basis as

$$|\Phi_j(\mathbf{R})\rangle = \sum_{\alpha}^{\text{N}_{\text{el}}} \sum_{n}^{\text{N}_{\text{F}}} \mathcal{C}_{\alpha,n}^j(\mathbf{R}) |\psi_\alpha(\mathbf{R}), n\rangle. \quad (4)$$

Here,  $\mathcal{C}_{\alpha,n}^j(\mathbf{R}) = \langle \psi_\alpha(\mathbf{R}), n | \Phi_j(\mathbf{R}) \rangle$ . The pQED method is systematically improvable, with convergence controlled by the number of included electronic  $N_{\text{el}}$  and photonic  $N_{\text{F}}$  states, and it has proven effective in capturing anisotropic cavity effects and light-induced modifications of molecular interactions.

In this work, we benchmark the performance of the pQED approach against the scQED-DFT-pMBD and scQED-CCSD (coupled cluster singles doubles – including two photonic excitations) approaches by investigating cavity-modified noncovalent interactions in model molecular systems. By systematically analyzing how cavity polarization, light-matter coupling strength, and basis convergence influence the predicted interaction energies, we assess the reliability and practicality of pQED-TDDFT relative to the state-of-the-art approaches, with benchmark calculations provided at the level

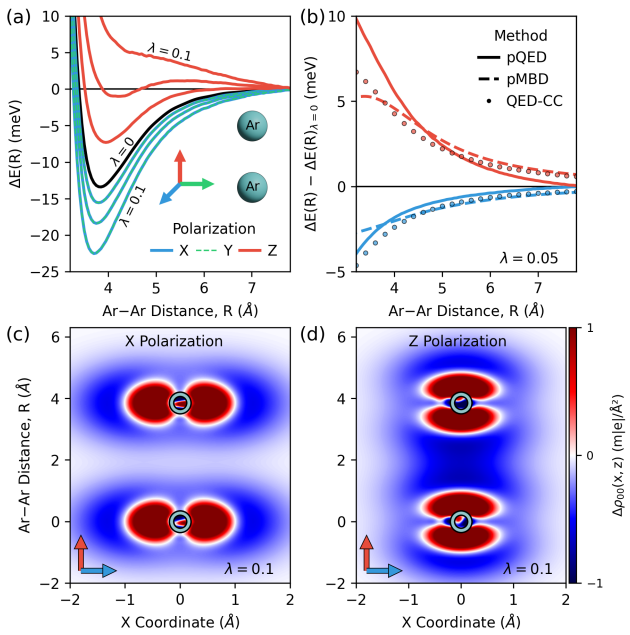


Figure 1: (a) Argon dimer ( $\text{Ar}_2$ ) potential energy surface,  $\Delta E(R) = E(R) - E(25\text{\AA})$ , outside (black) and inside cavity along different polarization directions X (solid blue), Y (dashed green), and Z (solid red) as functions of the dimer distance,  $R$ , along the Z-direction for  $\lambda = 0.000, 0.050, 0.075$  and  $0.100$  a.u. (b) Comparison of cavity-induced modifications to the potential energy surface,  $\Delta E(R, \lambda) - \Delta E(R, 0)$ , between the pQED-TDDFT, scQED-DFT-pMBD, and scQED-CC methods. Electronic Density difference ( $\Delta \rho_{00}(x, z) = \rho_{00}^M(x, z) - \xi_{00}(x, z)$ ) for (c) X and (d) Z-polarizations at the outside cavity equilibrium geometry ( $R \approx 3.85 \text{\AA}$ ), light blue circles indicate the atomic positions. In all panels, cavity frequency  $\omega_c = 2 \text{ eV}$ ,  $N_{\text{el}} = 431$  and  $N_F = 8$ . The scQED-DFT-pMBD and scQED-CC results were taken from Ref. 27. mention cavity frequency for the Ar

of scQED-CCSD. This comparison establishes the scope and limitations of current *ab initio* treatments of cavity-modified dispersion forces and provides a foundation for developing predictive theoretical tools in polaritonic chemistry.

## Results

### $\text{Ar}_2$ Dissociation

Figure 1 presents our first molecular system, which consists of an argon (Ar) dimer coupled to a single cavity mode. The internuclear direction of the two Ar atoms is parallel to the Z-axis (see inset in Figure 1a). Figure 1a shows the ground state potential energy surface,  $\Delta E(R) = E(R) - E(25\text{\AA})$ , as a function

of the interatomic distance the outside-cavity case (black curve) and for various cavity polarization directions X (blue), Y (green), and Z (red). When the cavity field is polarized along the Z-axis (along the internuclear bond), the Ar–Ar interaction is destabilized, and the cavity-modified potential energy surface becomes dissociative at large light-matter couplings  $\lambda = 0.1$  a.u. In contrast, polarization along the X- or Y-directions strengthens the attraction between the two Ar atoms by almost  $2\times$  (with X- and Y-directions producing identical effects due to symmetry of the molecular system).

Figure 1b shows the cavity-induced differences to the potential energy surface  $\Delta E(R, \lambda) - \Delta E(R, 0)$  between the inside- and outside-cavity cases for the pQED-TDDFT, scQED-DFT-pMBD, and scQED-CC approaches. The scQED-CC approach serves as a benchmark for the more approximate pQED-TDDFT and scQED-DFT-pMBD approaches, as it accurately captures non-covalent effects. The cluster operator in scQED-CC includes double excitations in the electronic space, double excitations in the photonic space, and coupled double excitations.<sup>28–30</sup> We note that the pQED-TDDFT and scQED-DFT-pMBD rely on the same exchange-correlation functional (PBE0) and basis set (aug-cc-pVDZ), with the only difference being that the pQED-TDDFT uses the Grimme D3 dispersion correction<sup>31</sup> while the scQED-DFT-pMBD does not.

To better understand the polaritonic effects on the electronic subsystem, we compute the electronic density difference  $\Delta \rho_{00}(x, z) = \rho_{00}^M(x, z) - \xi_{00}(x, z)$  (see c.a. Eq. 9 in **Theory** for more details). Visualization tools for electronic response are crucial for understanding many-body interactions.<sup>32–36</sup> Figure 1c,d presents these results. Here, positive values (red) indicate electron density accumulation, while negative values (blue) represent depletion. Similarly to Ref. 37, we find an overall contraction of the electronic density parallel to the cavity polarization direction, which is rationalized in the infinite coupling limit where the Hamiltonian (Eq. 1) becomes proportional to the molecular dipole operator and its square such that  $\lim_{\lambda \rightarrow \infty} \hat{H}_{\text{PF}} \sim \hat{\mu} + \hat{\mu}^2 \gg \hat{H}_{\text{el}}$ .

The contraction of the electronic density

along the cavity polarization axis  $\hat{\mathbf{e}}$  reduces the molecular polarizability tensor  $\alpha_{x_i x_j}$  in that direction  $\alpha_{ee}$ .<sup>17</sup> Using perturbation theory,<sup>17</sup> an expression for the cavity-modified vdW interaction energy is derived<sup>17</sup>

$$E_{\text{cvdW}}(R) = \frac{C_6}{R^3} \left( \cos^2(\theta) - \frac{1}{3} \right), \quad (5)$$

where  $C_6$  is the vdW coefficient and  $\theta = \arccos(\hat{\mathbf{e}} \cdot \hat{\mathbf{R}})$  is the angle between the cavity polarization unit vector  $\hat{\mathbf{e}}$  and the unit vector corresponding to the internuclear direction  $\hat{\mathbf{R}} = \frac{\vec{R}_1^{\text{COM}} - \vec{R}_2^{\text{COM}}}{|\vec{R}_1^{\text{COM}} - \vec{R}_2^{\text{COM}}|}$  with  $\vec{R}_i^{\text{COM}}$  as the vector corresponding to the center of mass (COM) of molecule  $i$ . X-polarization results in  $E_{\text{cvdW}}^{\hat{\mathbf{e}}=\mathbf{x}} = -\frac{C_6}{3R^3}$  while in the Z-polarization results in  $E_{\text{cvdW}}^{\hat{\mathbf{e}}=\mathbf{z}} = \frac{2C_6}{3R^3}$ , with the ratio  $\gamma_{xz} = \frac{|E_{\text{cvdW}}^{\hat{\mathbf{e}}=\mathbf{z}}|}{|E_{\text{cvdW}}^{\hat{\mathbf{e}}=\mathbf{x}}|} = 2$ . Looking at the potential energy surfaces in Figure 1a, it is clear that the Z-polarization results in stronger modifications compared to the X-polarization for the same light-matter coupling strength  $\lambda$ , further verified by examining Figure 1b. Figure S1 in **Supporting Information** presents the ratio of the cavity-modified potential energy surfaces for the X- and Z-polarizations, showing that at short internuclear distances the overlapping densities give rise to Dexter-like interactions (*i.e.*, non-vdW) but quickly converge to a ratio of 2.0 near  $R = 6 \text{ \AA}$  for the sQED-DFT-pMBD and scQED-CC approaches, while the pQED-TDDFT approach overestimates the energy ratio. Further, the pQED-TDDFT approach is noisy at large internuclear distances due to the ratio of small energies, and the error from lack of convergence is now a combined for the X- and Z-polarization as  $\sigma_{\text{ratio}} = \gamma_{xz} \sqrt{\left( \frac{\sigma_x}{|E_{\text{cvdW}}^{\hat{\mathbf{e}}=\mathbf{x}}|} \right)^2 + \left( \frac{\sigma_z}{|E_{\text{cvdW}}^{\hat{\mathbf{e}}=\mathbf{z}}|} \right)^2}$ . Thus, the pQED-TDDFT approach requires stricter convergence at large internuclear distances since the cavity-induced changes become small.

In Figure 1c, the X-polarized cavity compresses the electron cloud along the X-axis. We hypothesize that this contraction of the density effectively enhances the polarizability in the direction of the internuclear bond  $\alpha_{RR} = \alpha_{zz}$ . This cavity enhancement promotes stronger correlated density fluctuations between the Ar

atoms along the Z-direction, leading to an overall increase in attractive vdW interactions due to the negative energy contributions from the cvdW term in Eq. 5. In contrast, the Z-polarized cavity (Figure 1d) confines the electronic density along the intermolecular axis (Z-axis), suppressing the polarizability and diminishing correlated density fluctuations in that direction. As a result, the total dispersion energy is increased due to the positive contribution of the cvdW energy<sup>38</sup> (Eq. 5), weakening the internuclear bond and eventually leading to a completely repulsive interaction. This effect is a combination of the positive cvdW energy, as well as a now less screened electron-electron repulsion between the two interacting densities. Thus, the cavity polarization provides a tunable route toward systematic manipulation of the electronic subsystem.

As discussed earlier, the cavity mode can either enhance or deplete the electron density in the region between the two atoms, thereby modifying the strength of the non-covalent interaction. However, as the interatomic separation grows, the overlap of the electronic densities decreases, and, consequently, the cavity-induced redistribution of charge no longer significantly affects the interaction. This behavior can be observed in Figure 1b, where the pQED-TDDFT is in excellent agreement with the scQED-CC benchmark through the scanned distance for all polarization directions (in particular, along the X-polarization direction). In contrast, the scQED-DFT-pMBD method deviates at short Ar–Ar separations, specifically for the Z-polarization, where the scQED-DFT-pMBD approach exhibits a local maximum at  $R \approx 3 \text{ \AA}$ . This deviation arises because the pMBD approach primarily accounts for cavity-modified long-range dispersion and vdW interactions, while short-range exchange-repulsion effects – significant when the electronic densities overlap – are not included. Combining approaches at both short<sup>39</sup> and long range may yield more equal treatment of the full dispersion.<sup>27</sup>

The pQED method treats the number of electronic states ( $N_{\text{el}}$ ) and Fock states ( $N_{\text{F}}$ ) as convergence parameters.<sup>1,40,41</sup> Figure 2a,b show the

convergence of the total energy  $\Delta E(R_{\text{MIN}})$  at the minimum Ar-Ar separation outside the cavity,  $R_{\text{MIN}} \approx 1.85$  Å, as a function of  $N_{\text{el}}$  (Figure 1c) and  $N_{\text{F}}$  (Figure 1d). The zero-energy reference is taken as the maximum number of states,  $N_{\text{el}}^{\text{max}} = 431$  and  $N_{\text{F}} = 8$ . As a function of the number of electronic states (Figure 2a), the total energy is a non-monotonic function and stabilizes, to within 1 meV, around  $N_{\text{el}} = 200$ –300 electronic states for all three polarization directions. In contrast, the dependence on  $N_{\text{F}}$  (Figure 2b) is monotonic and converges, within 1 meV with two Fock states,  $N_{\text{F}} = 2$ . These findings indicate that the number of electronic states is the key parameter for achieving converged results from the pQED approach.<sup>41</sup>

Interestingly, the number of electronic states  $N_{\text{el}}$  needed to achieve convergence is also dependent on the nuclear configuration  $R$  of the system, as presented in Figure 2c,d, for the X- and Z-polarizations of the cavity, respectively. Here, the convergence of  $\Delta E(R)$  is evaluated at different Ar-Ar distances  $R$  and  $N_{\text{el}}$  and presented as a heatmap. Similarly to Figure 1c,d, the converged results are used as the reference as  $\Delta E(R, N_{\text{el}}) - \Delta E(R, N_{\text{el}}^{\text{conv.}})$  at each  $R$ . For the Ar-Ar case,  $N_{\text{el}}^{\text{Conv.}} = 431$ . Practically, this is represented as a value of zero for the top rows of each heatmap. Both polarizations show similar non-monotonic convergence as presented in Figure 1c for all nuclear configurations. At small internuclear distances  $R < 4$  Å, larger fluctuations occur, while for large separations  $R > 6$  Å, the fluctuations are reduced. This results from stronger short-range electronic correlations arising from enhanced wavefunction overlap between the argon atoms. It is also important to note that the colorbar scale is biased toward the positive (red), meaning that the majority of the large fluctuations lie above the converged energy.

## Water Dimer Dissociation

The second system we investigate is the dissociation of a water dimer. As shown in the inset of Figure 3a, the two molecules are arranged such that a hydrogen atom of one water molecule points toward the oxygen atom of the other

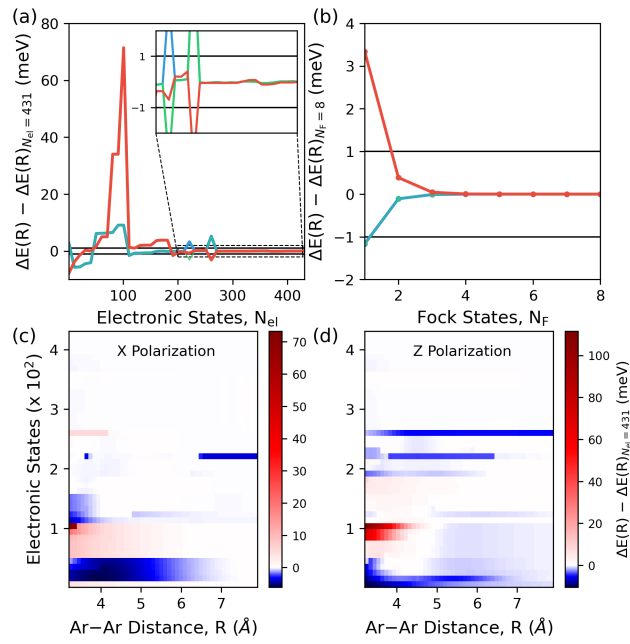


Figure 2: Convergence of  $\Delta E(R)$  for the pQED approach with respect to the number of (a) electronic states  $N_{\text{el}}$  and (b) Fock states  $N_{\text{F}}$  used in the construction of the polaritonic Hamiltonian at the equilibrium position ( $R \approx 3.7$  Å). Horizontal solid black lines indicate a threshold of 1 meV for comparison.  $\Delta E(R)$  as a function of Argon Dimer distance and  $N_{\text{el}}$  for (c) X and (d) Z polarizations. In panels (a,c,d)  $N_{\text{F}} = 8$ . In panel (b)  $N_{\text{el}} = 431$ . In all panels, cavity frequency  $\omega_c = 2$  eV and  $\lambda = 0.05$  a.u.

along the Z-direction, resulting in an interaction dominated by hydrogen bonding, which is mainly electrostatic. We note that hydrogen bonding interactions are much larger than the previously explored Ar-Ar vdW interaction by a factor of  $\sim 20$ . The potential energy surface ( $\Delta E(R) = E(R) - E(25\text{\AA})$ ) as a function of the hydrogen - oxygen distance ( $R$ ) is presented in Figure 3a for a single light-matter coupling strength  $\lambda = 0.05$  a.u. The cavity polarization along the X- and Y-directions stabilizes the water dimer by increasing the dissociation energy, thereby enhancing the strength of the hydrogen bond. In contrast, the Z-polarized cavity destabilizes the dimer by decreasing the dissociation energy, weakening the interaction.

This behavior can be understood by analyzing the electronic density difference  $\Delta\rho_{00}(x, z)$ . As in the case of the Ar dimer, the cavity field induces an anisotropic redistribution of the electronic density that depends on the polarization

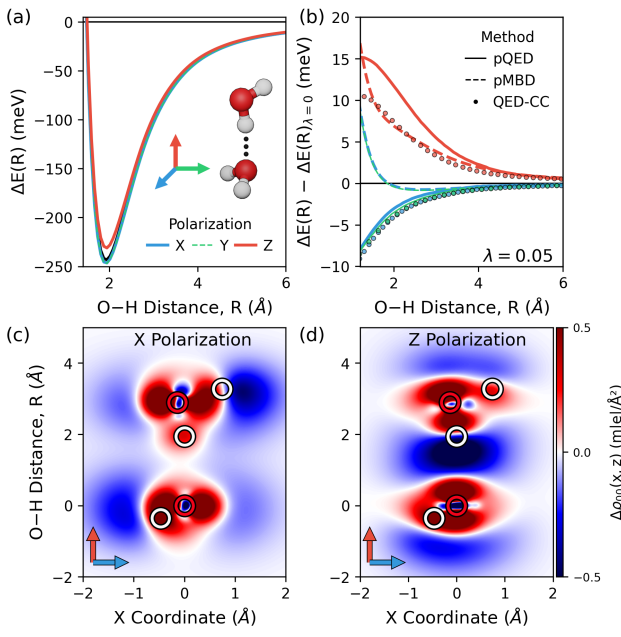


Figure 3: Water Dimer potential energy surface ( $\Delta E(R) = E(R) - E(25 \text{ \AA})$ ) outside (black) and inside (colors) cavity along different polarization directions. (a)  $\Delta E(R)$  as a function of the Dimer distance along the Z direction. (b) Inside cavity  $\Delta E(R)$  comparison between pQED-TDDFT, scQED-DFT-pMBD, and scQED-CC methods. Electronic Density difference ( $\Delta\rho_{00}(x, z) = \rho_{00}^M(x, z) - \xi_{00}(x, z)$ ) for (c) X and (d) Z polarizations at the outside cavity equilibrium geometry ( $R \approx 1.85 \text{ \AA}$ ), circles indicate the atomic positions color coded as the inset in (a). In all cases  $\Delta E(R) = E(R) - E(R=25 \text{ \AA})$ , cavity frequency  $\omega_c = 2 \text{ eV}$   $N_{\text{el}} = 720$  and  $N_F = 8$ . The scQED-DFT-pMBD and scQED-CC results were taken from Ref. 27.

direction. Under X-polarization (Figure 3c), the cavity field localizes the electron density closer to the atoms within each molecule. This redistribution enhances the polarizability of the dimer along the intermolecular direction (Z-axis), thereby strengthening the correlated density fluctuations that give rise to the attractive van der Waals interaction. In contrast, for Z polarization (Figure 3d), the electronic density becomes confined along the intermolecular axis, which suppresses the corresponding polarizability and weakens these correlated fluctuations. As the attractive dispersion contribution diminishes, electron-electron repulsion becomes dominant, resulting in a less stable configuration.

Analogously to Figure 1b, Figure 3b presents the difference in potential energy surfaces inside and outside the cavity  $\Delta E(R, \lambda) - \Delta E(R, 0)$ .

Here, the pQED-TDDFT approach (solid curves) closely matches the scQED-CC results (circles), reproducing the shapes of the curves for both polarizations. The X- and Y-polarizations are nearly quantitative, while the Z-polarization overestimates the value by  $\approx 30\%$ . However, the scQED-DFT-pMBD cannot reproduce the scQED-CC benchmark at short dimer separations R, even qualitatively. Further, the X- (dashed blue) and Y-polarizations (dashed green), in particular, have the wrong curvature. As discussed in Ref. 27, this is because the scQED-DFT-pMBD does not fully account for the local electrostatic effects that dominate the hydrogen dimer's behavior.

Convergence with respect to  $N_{\text{el}}$  and  $N_F$  for the water dimer at the equilibrium geometry  $R_{\min} = 1.8 \text{ \AA}$  of the dimer outside the cavity is shown in Figure 4a,b. The energy exhibits a similar non-monotonic dependence on the number of electronic states as in the Ar-Ar dimer (Figure 2a). The fluctuations stabilize to within  $\sim 1 \text{ meV}$  around  $N_{\text{el}} \approx 500$ . On the other hand, the Fock states reach convergence to within 1 meV at  $N_F = 2$ . Figures 4c,d further illustrate that the required number of electronic states  $N_{\text{el}}$  varies with the dimer separation. As before, a larger number of electronic states is needed at shorter intermolecular distances due to the increase in intermolecular wavefunction overlap between dimers.

## Slip Coordinate of the $\pi$ -stacked Benzene Dimer

We next analyze a benzene dimer, with the two molecules arranged in a parallel, stacked configuration at a constant separation of  $3.3 \text{ \AA}$  along the Z-axis (see inset of Figure 5a). The potential energy surface as a function of the intermolecular slip coordinate R (*i.e.*, the distance along the X-direction) is presented in Figure 5a. This motion, referred to as a slip plane, is important in designing and understanding molecular crystals.<sup>42</sup> From the perspective of intermolecular Kasha-like interactions, the stacking between monomers undergoes multiple transitions, between H- and J-aggregate-like aggre-

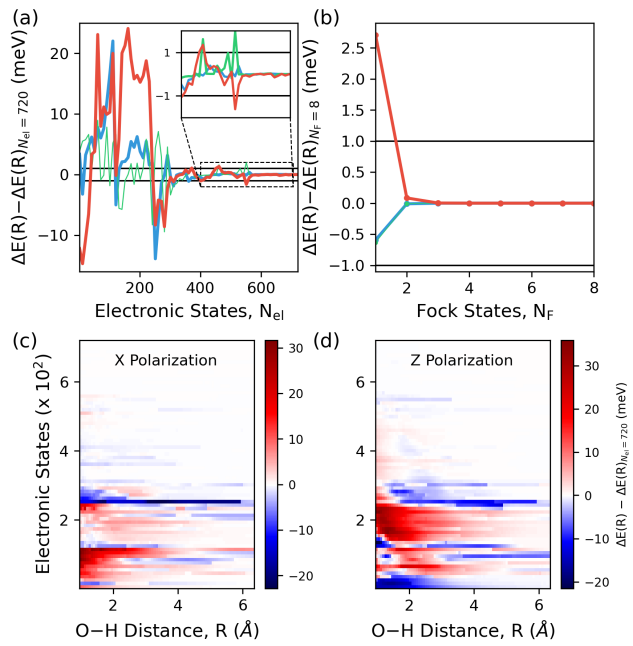


Figure 4: The dependence of the (a) number of electronic states  $N_{el}$  and (b) photonic Fock states  $N_F$  at the equilibrium position ( $R \approx 1.85 \text{ \AA}$ ).  $\Delta E(R)$  as a function of Water Dimer distance and  $N_{el}$  for (c) X- and (d) Z-polarizations. In all cases  $\Delta E(R) = E(R) - E(R=25 \text{ \AA})$ ,  $\lambda = 0.05 \text{ a.u.}$ , cavity frequency  $\omega_c = 2 \text{ eV}$ ,  $N_{el} = 720$ , and  $N_F = 8$

gates, as a function of the slip length.<sup>43,44</sup> We expect the cavity to induce modifications of these aggregate theories via manipulation of the local electronic density.

In the absence of the cavity (black curve), the system exhibits a minimum energy stacked configuration near  $R \approx 1.8 \text{ \AA}$ . When the cavity is introduced, the interaction becomes strongly polarization dependent, with energy modifications ranging from +70 meV for the Z-polarization to -50 for the Y-polarization. Polarization along the X-direction increases  $\Delta E(R)$  for most  $R$ , whereas the Y-direction lowers the energy for most  $R$ . However, both X- and Y-polarizations accentuate the minimum energy geometry at  $R \approx 1.9 \text{ \AA}$  by steepening the potential energy surface near  $R \approx 4 \text{ \AA}$ . In contrast, the Z-polarization increases  $\Delta E$  overall and induces the emergence of a new stable minimum at  $R \approx 4 \text{ \AA}$ .

The density-difference maps at the out-of-cavity equilibrium geometry ( $R \approx 1.8 \text{ \AA}$ ) are shown in Figures 5c,d. Under X-polarization (Fig. 5c), the cavity field compresses the charge

density (with blue indicating electron depletion and red electron accumulation) along the field direction and redistributes it onto the intramolecular bonds and weakly into the intermolecular space. The increased electron density in the intermolecular direction (Z) enhances the polarizability along this axis, which strengthens the dispersion interaction,<sup>27</sup> consistent with the stabilization observed in the potential energy surface. Notably, the magnitude of this density accumulation decreases with increasing slip distance, explaining why the attractive van der Waals contribution weakens at larger separations and why the interaction energy rises in this region (see Figure S3a,c).

For Z-polarization (Fig. 5d), the cavity localizes the electronic density onto the intramolecular  $\pi$ -orbitals, biased toward the negative Z-direction on each benzene molecule. The largest depletion of electron density occurs in the intermolecular space with a substantial reduction in the extra-molecular space (above the top molecule and below the bottom molecule). As discussed previously, this reduction in density between the benzene molecules suppresses the associated polarizability in that direction, thereby weakening the attractive vdW interaction. Interestingly, the density redistribution under Z-polarization varies only weakly along the slip coordinate, which explains the relatively flat energy landscape between 2 and 4  $\text{\AA}$  in Figure 5a (see Figure S3b,d). These results demonstrate that the cavity can both remove and introduce critical points in molecular potential energy surfaces of molecules and materials. Similar cavity-induced reshaping has been reported in excited-state energy landscapes, where avoided crossings can be strengthened or weakened to suppress or enable non-adiabatic transitions or to develop conical-intersection-like behavior without invoking changes to the polarization direction.<sup>40</sup> For cavity-induced ground state modifications, these results have strong implications for tuning thermally activated, cavity polarization-dependent reaction mechanisms.<sup>26,41</sup>

Figure 5b presents the comparison between the pQED-TDDFT and scQED-DFT-pMBD approaches. In this case, the scQED-CC results

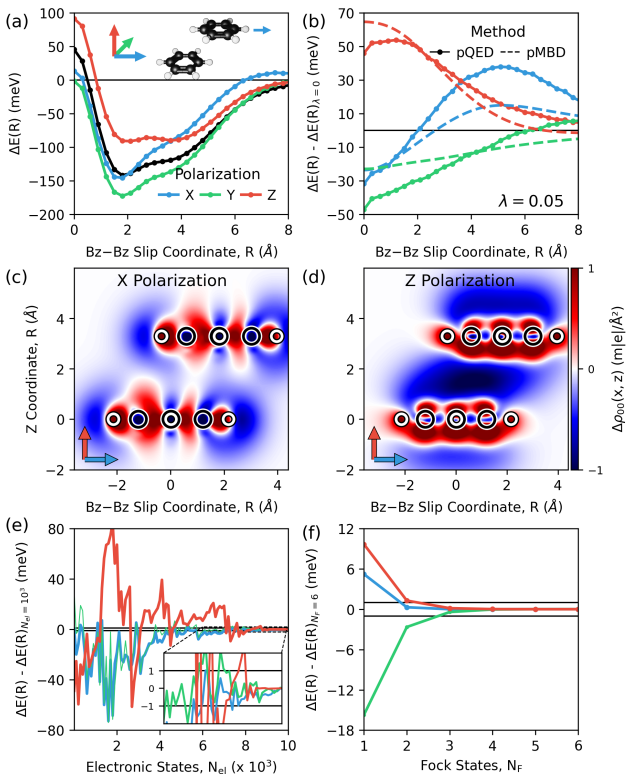


Figure 5: Benzene Dimer potential energy surface ( $\Delta E(R) = E(R) - E(25 \text{ \AA})$ ) outside (black) and inside (colors) cavity along different polarization directions. (a)  $\Delta E(R)$  as a function of the Dimer distance along the X direction. (b) Inside cavity  $\Delta E(R)$  comparison between the pQED-TDDFT and scQED-DFT-pMBD methods. Electronic Density difference ( $\Delta \rho_{00}(x, z) = \rho_{00}^M(x, z) - \xi_{00}(x, z)$ ) for (c) X and (d) Z polarizations at the outside cavity equilibrium geometry ( $R \approx 1.8 \text{ \AA}$ ), circles indicate the atomic positions color coded as the inset in (a).  $\Delta E(R)$  dependence on (e)  $N_{\text{el}}$  and (f)  $N_F$  at  $R \approx 1.8 \text{ \AA}$ . In all panels  $\Delta E(R) = E(R) - E(R=25 \text{ \AA})$ , light-matter coupling strength  $\lambda = 0.05$ , and cavity frequency  $\omega_c = 2 \text{ eV}$ . In panels (a)-(e)  $N_{\text{el}} = 10^4$  and in panel (a)-(d),(f)  $N_F = 6$ . The scQED-DFT-pMBD results were taken from Ref. 27.

were not reported in Ref. 27 due to the high computational cost. Both approaches, however, qualitatively agree on the cavity-induced modification of the potential energy surface,  $\Delta E(R, \lambda) - \Delta E(R, 0)$ , along the dimer slip distance  $R$ .

The convergence with respect  $N_{\text{el}}$  and  $N_F$  is shown in Figure 5e,f at a dimer distance of  $1.8 \text{ \AA}$ . Among all systems studied, this one exhibits the slowest convergence with respect to the number of electronic states  $N_{\text{el}}$ , and Fock states  $N_F$ . Convergence within 1 meV is reached at  $N_{\text{el}} = 8000$  and  $N_F = 3$ . This

slow convergence likely arises from the large number of possible electronic transitions in the system and from the highly conjugated nature of both monomers, which support strong intramolecular (*e.g.*,  $\pi-\pi^*$ ) and inter-molecular (*e.g.*, charge transfer) dipole transitions. The significant energy change observed between  $N_F = 1$  and  $N_F = 6$  ( $\sim 10 \text{ meV}$ ) reflects the dense manifold of electronic states that, within the cavity, couple more strongly and therefore require a larger number of cavity-dressed basis functions to resolve. For all other systems investigated in this work, the variation in energy with respect to Fock-state convergence remains below 5 meV. The convergence scan along the slipping coordinate  $R$  was not performed for this system due to the large computational expense.

## Benzene – Argon Dissociation

As a final example, we studied the dissociation of the Benzene-Ar complex, which is primarily by weak vdW interactions. As illustrated in the inset of Figure 6a, the benzene ring lies in the XY-plane and centered along the Z-axis, with the Ar atom positioned above the ring along this same axis. Figure 6a displays the potential energy surface,  $\Delta E(R) = E(R) - E(25 \text{ \AA})$ , as a function of the Benzene-Ar distance  $R$  for a light-matter coupling strength  $\lambda = 0.05 \text{ a.u.}$  and cavity frequency  $\omega_c = 2.0 \text{ eV}$ . In close analogy with the other systems examined in this work, cavity polarization in the X- and Y-directions yields a similar extent of stabilization of the complex ( $\sim 10 \text{ meV}$ ). In contrast, Z-polarization, which is aligned with the intermolecular axis, produces destabilization ( $\sim 20 \text{ meV}$ ).

To elucidate the microscopic origin of these trends, we computed the electronic density difference of the ground state ( $\Delta \rho_{00}(x, z)$ ) at the out-of-cavity equilibrium geometry ( $R \approx 3.2 \text{ \AA}$ ). For the X-polarization (Figure 6c), the cavity field constrains electronic density along the polarization axis, driving a redistribution of charge into (red) the intramolecular bonds of the benzene as well as to a  $p_x$ -like orbital closer to the Ar atom. At the center of the benzene ring, the accumulation (red) leaks into

the intermolecular space. This results in a net accumulation of density along the intermolecular coordinate, thereby enhancing the longitudinal polarizability and amplifying the correlated density fluctuations that give rise to dispersion.<sup>27</sup> The strengthened vdW interaction in the parallel direction as the intermolecular bond accounts for the increased stabilization observed in Figure 6a (see Eq. 5). In contrast, under Z-polarization (Figure 6d), the electron density is drawn from the intermolecular space as well as below the benzene ring and accumulated nearly uniformly on the carbon atoms. This redistribution diminishes the polarizability, reducing the attractive dispersion interaction. These results are consistent with the cavity-modified interaction predicted by Eq. 5.

Figure 6b present the difference in potential energy surfaces inside and outside the cavity ( $\Delta E(R, \lambda) - \Delta E(R, 0)$ ) for the three *ab initio* polaritonic-structure approaches considered. In all three cases of cavity polarization directions, the pQED-TDDFT results are in excellent agreement with the scQED-CC benchmark. For the X- and Y-polarizations, the scQED-DFT-pMBD method fails to reproduce the correct short-range behavior. In contrast, for the Z-polarization, the scQED-DFT-pMBD closely follows the scQED-CC reference. Even though the pQED-TDDFT approach qualitatively captures the Z-polarization, it exhibits a slight deviation at short intermolecular separations, where it does not capture the location of the maximum.

Finally, Figure 6e,f present the convergence of the molecular system energy at the outside cavity equilibrium geometry  $R \approx 3.2 \text{ \AA}$  with respect to the number of electronic states  $N_{\text{el}}$  and Fock states  $N_F$ . As in previous systems, we observe a non-monotonic convergence pattern with  $N_{\text{el}}$ , which stabilizes to within 1 meV at around 3000 states, while convergence with respect to the photonic subspace is achieved monotonically by  $N_F = 2$ .

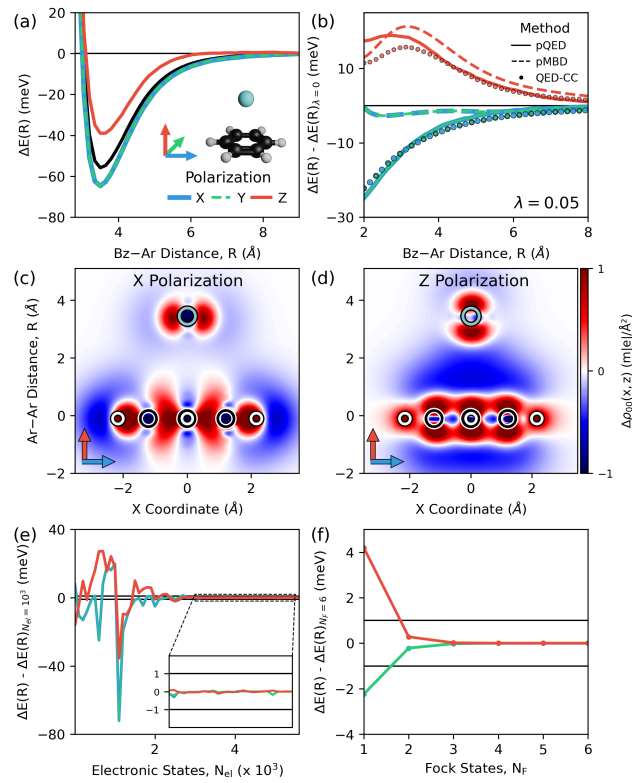


Figure 6: (a) Benzene-Ar potential energy surface,  $\Delta E(R) = E(R) - E(25 \text{ \AA})$ , outside (black) and inside (colors) the cavity along different polarization directions. (b) Difference in potential energy surfaces inside and outside the cavity,  $\Delta E(R, \lambda) - \Delta E(R, 0)$  for the pQED-TDDFT (solid), scQED-DFT-pMBD (dashed), and scQED-CC (circles) methods. Electronic Density difference ( $\Delta \rho_{00}(x, z) = \rho_{00}^M(x, z) - \xi_{00}(x, z)$ ) for (c) X- and (d) Z-polarizations at the outside cavity equilibrium geometry ( $R \approx 3.2 \text{ \AA}$ ), circles indicate the atomic positions color coded as the inset in (a). Only one set of eclipsed C and H atoms is shown. Convergence of the potential energy at the minimum energy geometry outside the cavity  $\Delta E(R_{\min} = 3.2 \text{ \AA})$  with respect to (e) the number of electronic state  $N_{\text{el}}$  and (f) Fock states  $N_F$ . In all panels  $\Delta E(R) = E(R) - E(R = 25 \text{ \AA})$ , light-matter coupling strength  $\lambda = 0.05 \text{ a.u.}$ , and cavity frequency  $\omega_c = 2.0 \text{ eV}$ . In panels (a)-(e)  $N_{\text{el}} = 4000$  and in panels (a)-(d),(f)  $N_F = 10$ . The scQED-DFT-pMBD and scQED-CC results were taken from Ref. 27.

## Conclusions

In this work, we have presented a systematic investigation of cavity-modified non-covalent interactions in the polaritonic ground state using the parameterized quantum electrodynamics (pQED) approach based on time-dependent density functional theory (pQED-TDDFT).<sup>26,40,41</sup> In applying pQED-TDDFT to argon and water dimers as well as to benzene-based aggre-

gates, we demonstrated its ability to capture the anisotropic (cavity polarization-dependent) modifications to intermolecular potentials induced by strong light–matter coupling. Inspired by recent progress in developing state-of-the-art exchange-correlation functionals for cavity QED, we benchmarked the pQED-TDDFT results against reported high-level self-consistent QED coupled cluster (scQED-CC) calculations developed in Ref. 45 as well as to the self-consistent photon many-body dispersion exchange-correlation functional for cavity QED density functional theory (scQED-DFT-pMBD) developed in Ref. 27.

Our findings show that both the pQED-TDDFT and scQED-DFT-pMBD reproduce the qualitative and often quantitative trends of cavity-modified potential energy surfaces of the polaritonic ground state with good agreement to correlated benchmarks (scQED-CC). The scQED-DFT-pMBD does exhibit limitations in systems dominated by local electrostatics (Figure 3) as well as in certain cavity polarization directions for induced dipole interactions (Figure 6).

To quantitatively understand how the cavity modifies the intermolecular interactions, we computed the ground-state electronic density difference, and this revealed that the cavity-induced density redistribution governs the changes to the intermolecular interaction energy. Specifically, we observed electron density localization parallel to the cavity polarization direction. This cavity-mediated redistribution directly impacts stability by inducing electron density depletion in the intermolecular region which decreases van der Waals (vdW) interaction energy. In contrast, accumulation of electronic density increases the stabilization. While further studies are needed, we propose that these observations can be understood from changes in molecular polarizability along the intermolecular axis, induced by the shifting electron density.<sup>17</sup>

In all model systems explored in this work, we explicitly tested the convergence properties of the pQED-TDDFT approach. As discussed briefly in previous works,<sup>40,41</sup> the convergence of pQED-TDDFT for ground state properties is more expensive than for excited states due to the necessity of increased strong light-matter coupling  $\lambda$  for ground state modifications. Another complications is that the ground polaritonic state is dominated by the dipole self-energy.<sup>26,41</sup> The sum-over-states approach used in this work to calculate the molecular dipole self-energy term in the Hamiltonian,

$\hat{H}_{\text{DSE}} \propto \hat{\mu}^2 = \sum_{\alpha} \hat{\mu} |\psi_{\alpha}(\mathbf{R})\rangle \langle \psi_{\alpha}(\mathbf{R})| \hat{\mu}$ , is known to be difficult to converge.<sup>46–48</sup> However, for small-to-medium systems of interest, the pQED-TDDFT approach can be readily applied to investigate the polaritonic ground state, often providing excellent agreement with coupled cluster results<sup>40</sup> and with reliable, but often slow, convergence in all systems explored to date.<sup>41</sup>

## Theory

The formulation of the light–matter Hamiltonian and the underlying principles of the pQED-TDDFT approach were introduced in Section (Eqs. 1–3). Building upon this, we now highlight two physically distinct yet complementary mechanisms through which the ground polaritonic state can be modified, even when the cavity is off-resonant with the bright electronic excitations. First, the bilinear light–matter interaction term in Eq. 1 induces mixing between electronic and photonic manifolds even in the off-resonant cases. For example, the state  $|\psi_g, 0\rangle$  couples to  $|\psi_g, 1\rangle$  through the matrix element  $\langle \psi_g, 0 | \hat{\mu} (\hat{a}^\dagger + \hat{a}) | \psi_g, 1 \rangle = \mu_{gg} \langle 0 | (\hat{a}^\dagger + \hat{a}) | 1 \rangle = \mu_{gg}$ . Similarly, the state  $|\psi_g, 1\rangle$  couples  $|\psi_e, 0\rangle$  through  $\langle \psi_e, 0 | \hat{\mu} (\hat{a}^\dagger + \hat{a}) | \psi_g, 1 \rangle = \mu_{ge} \langle 0 | (\hat{a}^\dagger + \hat{a}) | 1 \rangle = \mu_{ge}$ , where  $\mu_{gg}$  and  $\mu_{ge}$  are the permanent and transition dipoles. While each individual off-resonant matrix element is small, the cumulative contribution from many such virtual excitations leads to a renormalization of the electronic ground state and introduces a small but nonzero photonic component into  $|\psi_g, 0\rangle$ . Second, and typically more significant for the ground state energy, the dipole self energy (DSE) provides a quadratic, all-to-all electronic coupling channel through  $(\hat{\mu} \cdot \hat{\mathbf{e}})^2 = \hat{\mu}^2$  where we denote  $\hat{\mu}$  as the projection of  $\hat{\mu}$  along the cavity polarization direction  $\hat{\mathbf{e}}$ . The DSE couples the ground state  $|\psi_g\rangle$  to every electronic state  $|\psi_{\alpha}\rangle$  through the matrix elements  $\langle \psi_g | \hat{\mu}^2 | \psi_{\alpha} \rangle = \sum_{\gamma} \mu_{g\gamma} \mu_{\gamma\alpha}$ , where  $\alpha$  and  $\gamma$  run over all excited states. This collective coupling channel often represents the dominant cavity-induced modification of the ground-state energy.

Having established these mechanisms, we introduce the density-difference formalism used to analyze the resulting changes in the ground-state electronic structure. The density difference is defined

as:

$$\Delta\rho_{00}(\mathbf{R}) = \rho_{00}^M(\mathbf{R}) - \xi_{00}(\mathbf{R}) \quad (6)$$

Here,  $\rho_{00}^M(\mathbf{R})$  is the polaritonic density where the photonic DOFs have been traced out,

$$\begin{aligned} \hat{\rho}_{00}^M(\mathbf{R}) &= \text{Tr}_{\text{ph}} [\hat{\rho}_{00}(\mathbf{R})] = \text{Tr}_{\text{ph}} [|\Phi_0(\mathbf{R})\rangle\langle\Phi_0(\mathbf{R})|] \\ &= \sum_{\alpha,\beta}^{N_{\text{el}}} \sum_n^{N_F} \mathcal{C}_{\alpha,n}^0(\mathbf{R}) \mathcal{C}_{\beta,n}^0(\mathbf{R}) \hat{\xi}_{\alpha\beta}(\mathbf{R}). \end{aligned} \quad (7)$$

where the orthogonality of the Fock states,  $\langle n|m \rangle = \delta_{n,m}$ , has been used. Here,

$$\begin{aligned} \xi_{\alpha\beta}(\mathbf{R}, \mathbf{r}_1, \mathbf{r}'_1) &= \\ &\int d\mathbf{r}_2 \cdots d\mathbf{r}_{n_e} d\mathbf{r}'_2 \cdots d\mathbf{r}'_{n_e} \\ &\times \langle \mathbf{r}_1 \cdots \mathbf{r}_{n_e} | \psi_\alpha \rangle \langle \psi_\beta | \mathbf{r}_1 \cdots \mathbf{r}_{n_e} \rangle \end{aligned} \quad (8)$$

is the one-particle transition density operator between electronic states  $\alpha$  and  $\beta$  where  $n_e$  is the number of electrons. Also note that  $(\mathcal{C}_{\alpha,n}^0)^* = \mathcal{C}_{\alpha,n}^0$  since the Hamiltonian is real-valued. In principle, the polaritonic density is composed of all possible one-particle electronic density matrices, including state densities  $\xi_{\alpha\alpha}(\mathbf{r})$ , ground-to-excited transition densities  $\xi_{0\alpha}(\mathbf{r})$  and  $\xi_{\alpha 0}(\mathbf{r})$ , and excited-to-excited transition densities  $\xi_{\alpha\beta}(\mathbf{r})$ . However, we only consider the ground-to-excited transition density as these will present the largest contributions.<sup>15</sup> The integrated density difference was computed as,

$$\Delta\rho_{00}(x, z) = \int dy \cdot \Delta\rho_{00}(x, y, z). \quad (9)$$

The full electronic density difference ( $\Delta\rho_{00}(x, z)$ ) for all systems studied in this work are presented in Figure S5 and Figure S6 of the Supporting Information

## Computational Details

All electronic structure calculations were performed using the Gaussian 16 software.<sup>49</sup> We used the pQED time-dependent density functional theory (pQED-TDDFT) approach with the PBE0 hybrid functional along with the aug-cc-pVDZ basis set. To account for the long-range dispersion interactions (London dispersion and van Der Waals forces), we employed Grimme's D3 empirical dispersion correction<sup>31</sup> (Figure S4 of the Supporting Information presents the inside and outside cavity results when the dispersion forces are not con-

sidered). Unless otherwise stated, the molecular systems are coupled to a single cavity mode with frequency  $\omega_c = 2$  eV and light-matter coupling  $\lambda = 0.05$  a.u.

For a given cavity polarization direction,  $\hat{\mathbf{e}}$ , we use the matrix elements of the projected dipole operator,  $\mu_{\alpha\beta}(\mathbf{R}) = \langle \psi_\alpha(\mathbf{R}) | \hat{\mathbf{\mu}} \cdot \hat{\mathbf{e}} | \psi_\beta(\mathbf{R}) \rangle$ , obtained from the electronic structure calculations. Further, to compute the dipole self energy term, we employ a sum-over-states-like approach<sup>46–48</sup> for the square of the molecular dipole operator as,  $(\hat{\mu}^2)_{\alpha\beta} = \sum_\gamma \langle \psi_\alpha(\mathbf{R}) | \hat{\mathbf{\mu}} \cdot \hat{\mathbf{e}} | \psi_\gamma(\mathbf{R}) \rangle \langle \psi_\gamma(\mathbf{R}) | \hat{\mathbf{\mu}} \cdot \hat{\mathbf{e}} | \psi_\beta(\mathbf{R}) \rangle = \sum_\gamma \mu_{\alpha\gamma} \mu_{\gamma\beta}$ , where  $\gamma$  runs over all possible electronic states. To avoid the full diagonalization of the light-matter Hamiltonian (Eq. 1), we performed a partial diagonalization using the Lanczos algorithm<sup>50–54</sup> as implemented in the scipy python package to get the lowest eigenvalue of the polaritonic system. Finally, to reduce the number of Fock States needed to achieve convergence, a coherence state shift is performed according to  $\hat{\mu}' = \hat{\mu} - \mu_{00} \cdot I_{el}$ , which is a unitary transformation on the Hamiltonian, preserving both eigenvalues and eigenvectors in a complete basis.<sup>28</sup>

**Acknowledgement** This work was supported by the Air Force Office of Scientific Research under AFOSR Award No. FA9550-23-1-0438. The software development for molecular polariton calculations in this work was partially supported by the National Science Foundation's Office of Advanced Cyberinfrastructure under Award No. OAC-2311442. S.M.V. appreciates the support of the Elon Huntington Hooker Fellowship from the University of Rochester. B.M.W. appreciates the support of the Director's Postdoctoral Fellowship at Los Alamos National Laboratory (LANL) as well as the Laboratory Directed Research and Development (LDRD) at LANL. LANL is operated by Triad National Security, LLC, for the National Nuclear Security Administration of the US Department of Energy (Contract No. 89233218CNA000001). Computing resources were provided by the Center for Integrated Research Computing (CIRC) at the University of Rochester, as well as Institutional Computing (IC) at LANL.

# Supporting Information Available

## References

- (1) Mandal, A.; Taylor, M. A. D.; Weight, B. M.; Koessler, E. R.; Li, X.; Huo, P. Theoretical Advances in Polariton Chemistry and Molecular Cavity Quantum Electrodynamics. *Chemical Reviews* **2023**, *123*, 9786–9879.
- (2) Dunkelberger, A. D.; Simpkins, B. S.; Vurgaftman, I.; Owrusky, J. C. Vibration-Cavity Polariton Chemistry and Dynamics. *Annual Review of Physical Chemistry* **2022**, *73*, 429–451.
- (3) Hirai, K.; Hutchison, J. A.; Uji-i, H. Molecular Chemistry in Cavity Strong Coupling. *Chemical Reviews* **2023**, *123*, 8099–8126.
- (4) Zeng, H.; Pérez-Sánchez, J. B.; Eckdahl, C. T.; Liu, P.; Chang, W. J.; Weiss, E. A.; Kalow, J. A.; Yuen-Zhou, J.; Stern, N. P. Control of Photoswitching Kinetics with Strong Light–Matter Coupling in a Cavity. *Journal of the American Chemical Society* **2023**, *145*, 19655–19661.
- (5) Freixas, V. M.; Malone, W.; Li, X.; Song, H.; Negrin-Yuvero, H.; Pérez-Castillo, R.; White, A.; Gibson, T. R.; Makhov, D. V.; Shalashilin, D. V. et al. NEXMD v2.0 Software Package for Nonadiabatic Excited State Molecular Dynamics Simulations. *Journal of Chemical Theory and Computation* **2023**, *19*, 5356–5368.
- (6) Mandal, A.; Krauss, T. D.; Huo, P. Polariton-Mediated Electron Transfer via Cavity Quantum Electrodynamics. *The Journal of Physical Chemistry B* **2020**, *124*, 6321–6340.
- (7) Lee, I.; Melton, S. R.; Xu, D.; Delor, M. Controlling molecular photoisomerization in photonic cavities through polariton funneling. *Journal of the American Chemical Society* **2024**, *146*, 9544–9553.
- (8) Ng, C.; Dligatch, S.; Amekura, H.; Davis, T. J.; Gómez, D. E. Waveguide-Plasmon Polariton Enhanced Photochemistry. *Advanced Optical Materials* **2015**, *3*, 1582–1590.
- (9) Koessler, E. R.; Mandal, A.; Musser, A. J.; Krauss, T. D.; Huo, P. Polariton mediated electron transfer under the collective molecule–cavity coupling regime. *Chemical Science* **2025**, *16*, 11644–11658.
- (10) Du, M.; Martínez-Martínez, L. A.; Ribeiro, R. F.; Hu, Z.; Menon, V. M.; Yuen-Zhou, J. Theory for Polariton-Assisted Remote Energy Transfer. *Chemical Science* **2018**, *9*, 6659–6669.
- (11) Thanh Phuc, N. Super-reaction: The collective enhancement of a reaction rate by molecular polaritons in the presence of energy fluctuations. *The Journal of Chemical Physics* **2021**, *155*.
- (12) Mandal, A.; Taylor, M. A.; Huo, P. Theory for cavity-modified ground-state reactivities via electron–photon interactions. *The Journal of Physical Chemistry A* **2023**, *127*, 6830–6841.
- (13) Flick, J.; Schäfer, C.; Ruggenthaler, M.; Appel, H.; Rubio, A. Ab initio optimized effective potentials for real molecules in optical cavities: Photon contributions to the molecular ground state. *ACS photonics* **2018**, *5*, 992–1005.
- (14) Haugland, T. S.; Ronca, E.; Kjønstad, E. F.; Rubio, A.; Koch, H. Coupled cluster theory for molecular polaritons: Changing ground and excited states. *Physical Review X* **2020**, *10*, 041043.
- (15) Weight, B. M.; Weix, D. J.; Tonzetich, Z. J.; Krauss, T. D.; Huo, P. Cavity quantum electrodynamics enables para-and ortho-selective electrophilic bromination of nitrobenzene. *Journal of the American Chemical Society* **2024**, *146*, 16184–16193.
- (16) Philbin, J. P.; Haugland, T. S.; Ghosh, T. K.; Ronca, E.; Chen, M.; Narang, P.; Koch, H. Molecular van der Waals Fluids in Cavity Quantum Electrodynamics. *The Journal of Physical Chemistry Letters* **2023**, *14*, 8988–8993.
- (17) Haugland, T. S.; Philbin, J. P.; Ghosh, T. K.; Chen, M.; Koch, H.; Narang, P. Understanding the polaritonic ground state in cavity quantum electrodynamics. *The Journal of Chemical Physics* **2025**, *162*, 194106.

- (18) Haugland, T. S.; Schäfer, C.; Ronca, E.; Rubio, A.; Koch, H. Intermolecular interactions in optical cavities: An ab initio QED study. *The Journal of Chemical Physics* **2021**, *154*, 094113.
- (19) Ruggenthaler, M.; Flick, J.; Pellegrini, C.; Appel, H.; Tokatly, I. V.; Rubio, A. Quantum-electrodynamical density-functional theory: Bridging quantum optics and electronic-structure theory. *Physical Review A* **2014**, *90*, 012508.
- (20) Flick, J.; Ruggenthaler, M.; Appel, H.; Rubio, A. Kohn–Sham approach to quantum electrodynamical density-functional theory: Exact time-dependent effective potentials in real space. *Proceedings of the National Academy of Sciences* **2015**, *112*, 15285–15290.
- (21) Mordovina, U.; Bunney, C.; Appel, H.; Knowles, P. J.; Rubio, A.; Manby, F. R. Polaritonic coupled-cluster theory. *Physical Review Research* **2020**, *2*, 023262.
- (22) Vu, N.; Mejia-Rodriguez, D.; Bauman, N. P.; Panyala, A.; Mutlu, E.; Govind, N.; Foley IV, J. J. Cavity quantum electrodynamics complete active space configuration interaction theory. *Journal of Chemical Theory and Computation* **2024**, *20*, 1214–1227.
- (23) McTague, J.; Foley, J. J. Non-Hermitian cavity quantum electrodynamics–configuration interaction singles approach for polaritonic structure with ab initio molecular Hamiltonians. *The Journal of chemical physics* **2022**, *156*.
- (24) Weight, B. M.; Tretiak, S.; Zhang, Y. Diffusion quantum Monte Carlo approach to the polaritonic ground state. *Physical Review A* **2024**, *109*, 032804.
- (25) Weber, L.; Dos Anjos Cunha, L.; Morales, M. A.; Rubio, A.; Zhang, S. Phaseless Auxiliary-Field Quantum Monte Carlo Method for Cavity-QED Matter Systems. *Journal of Chemical Theory and Computation* **2025**, *21*, 2909–2917.
- (26) Wang, J.; Weight, B. M.; Huo, P. Investigating Cavity Quantum Electrodynamics-Enabled Endo/Exo-Selectivities in a Diels–Alder Reaction. *The Journal of Physical Chemistry A* **2025**, *129*, 5458–5468.
- (27) Tasci, C.; Cunha, L. A.; Flick, J. Photon Many-Body Dispersion: Exchange-Correlation Functional for Strongly Coupled Light-Matter Systems. *Physical Review Letters* **2025**, *134*.
- (28) Haugland, T. S.; Ronca, E.; Kjønstad, E. F.; Rubio, A.; Koch, H. Coupled Cluster Theory for Molecular Polaritons: Changing Ground and Excited States. *Physical Review X* **2020**, *10*, 041043.
- (29) Foley, J. J., IV; McTague, J. F.; DePrince, A. E., III Ab initio methods for polariton chemistry. *Chemical Physics Reviews* **2023**, *4*, 041301.
- (30) Mordovina, U.; Bunney, C.; Appel, H.; Knowles, P. J.; Rubio, A.; Manby, F. R. Polaritonic coupled-cluster theory. *Physical Review Research* **2020**, *2*, 023262.
- (31) Grimme, S.; Antony, J.; Ehrlich, S.; Krieg, H. A consistent and accurate ab initio parametrization of density functional dispersion correction (DFT-D) for the 94 elements H–Pu. *The Journal of Chemical Physics* **2010**, *132*, 154104.
- (32) Weight, B.; Freixas, V.; Forde, A.; Tretiak, S. A Visual Understanding of Circular Dichroism Spectroscopy. <https://chemrxiv.org/engage/chemrxiv/article-details/6915246def936fb4a2db40df>, ChemRxiv, 2025, 10.26434/chemrxiv-2025-rv1vb.
- (33) Plasser, F.; Krylov, A. I.; Dreuw, A. libwfa: Wavefunction analysis tools for excited and open-shell electronic states. *WIREs Computational Molecular Science* **2022**, *12*, e1595, [eprint: https://wires.onlinelibrary.wiley.com/doi/pdf/10.1002/wcms.1595](https://wires.onlinelibrary.wiley.com/doi/pdf/10.1002/wcms.1595)
- (34) Plasser, F.; Bäppler, S. A.; Wormit, M.; Dreuw, A. New tools for the systematic analysis and visualization of electronic excitations. II. Applications. *J. Chem. Phys.* **2014**, *141*.
- (35) Plasser, F.; Wormit, M.; Dreuw, A. New tools for the systematic analysis and visualization of electronic excitations. I. Formalism. *J. Chem. Phys.* **2014**, *141*.

- (36) Freixas, V. M.; Rouxel, J. R.; Tretiak, S.; Govind, N.; Mukamel, S. Chiral population analysis: a real space visualization of X-ray circular dichroism. *Chemical Science* **2025**, *16*, 16218–16224.
- (37) Weight, B. M.; Tretiak, S.; Zhang, Y. Diffusion quantum Monte Carlo approach to the polaritonic ground state. *Physical Review A* **2024**, *109*, 032804.
- (38) Cairano, L. D.; Gori, M.; Karimpour, R.; Tkatchenko, A. Repulsive Inverse-Distance Interatomic Interaction from Many-Body Quantum Electrodynamics. <http://arxiv.org/abs/2511.08069>.
- (39) Flick, J. Simple Exchange-Correlation Energy Functionals for Strongly Coupled Light-Matter Systems Based on the Fluctuation-Dissipation Theorem. *129*, 143201.
- (40) Weight, B. M.; Krauss, T. D.; Huo, P. Investigating Molecular Exciton Polaritons Using Ab Initio Cavity Quantum Electrodynamics. *The Journal of Physical Chemistry Letters* **2023**, *14*, 5901–5913.
- (41) Weight, B. M.; Weix, D. J.; Tonzetich, Z. J.; Krauss, T. D.; Huo, P. Cavity Quantum Electrodynamics Enables para- and ortho-Selective Electrophilic Bromination of Nitrobenzene. *Journal of the American Chemical Society* **2024**, *146*, 16184–16193.
- (42) He, X.; Zhang, Z.; Zhang, C.; Niu, L. Identifying Possible Slip Systems of Molecular Crystals via a Geometry-Based Procedure. *Crystal Growth & Design* **2024**, *24*, 4342–4356.
- (43) Hestand, N. J.; Spano, F. C. Molecular Aggregate Photophysics beyond the Kasha Model: Novel Design Principles for Organic Materials. *Accounts of Chemical Research* **2017**, *50*, 341–350.
- (44) Hestand, N. J.; Spano, F. C. Expanded Theory of H- and J-Molecular Aggregates: The Effects of Vibronic Coupling and Intermolecular Charge Transfer. *Chemical Reviews* **2018**, *118*, 7069–7163.
- (45) Pavošević, F.; Hammes-Schiffer, S.; Rubio, A.; Flick, J. Cavity-Modulated Proton Transfer Reactions. *Journal of the American Chemical Society* **2022**, *144*, 4995–5002.
- (46) Jones, M.; Tennyson, J. On the Use of Pseudostates to Calculate Molecular Polarizabilities. *Journal of Physics B: Atomic, Molecular and Optical Physics* **2010**, *43*, 045101.
- (47) Otero, N.; Karamanis, P.; Mandado, M. A New Method to Analyze and Understand Molecular Linear and Nonlinear Optical Responses *via* Field-Induced Functions: A Straightforward Alternative to Sum-over-States (SOS) Analysis. *Physical Chemistry Chemical Physics* **2019**, *21*, 6274–6286.
- (48) Dalgarno, A.; Ford, A. L.; Browne, J. C. Direct Sum-of-States Calculations of the Frequency-Dependent Polarizability of H 2. *Physical Review Letters* **1971**, *27*, 1033–1036.
- (49) Frisch, M. J.; Trucks, G. W.; Schlegel, H. B.; Scuseria, G. E.; Robb, M. A.; Cheeseman, J. R.; Scalmani, G.; Barone, V.; Petersson, G. A.; Nakatsuji, H. et al. Gaussian 16. 2016; Gaussian Inc. Wallingford CT.
- (50) Lanczos, C. An iteration method for the solution of the eigenvalue problem of linear differential and integral operators. *Journal of research of the National Bureau of Standards* **1950**, *45*, 255–282.
- (51) Saad, Y. *Numerical Methods for Large Eigenvalue Problems*, revised edition ed.; Society for Industrial and Applied Mathematics: Philadelphia, PA, 2011.
- (52) Van Loan, C. F.; Golub, G. Matrix computations (Johns Hopkins studies in mathematical sciences). *Matrix Computations* **1996**, *5*, 32.
- (53) Tretiak, S.; Mukamel, S. Density matrix analysis and simulation of electronic excitations in conjugated and aggregated molecules. *Chemical reviews* **2002**, *102*, 3171–3212.
- (54) Tretiak, S.; Isborn, C. M.; Niklasson, A.; Challacombe, M. Representation independent algorithms for molecular response calculations in time-dependent self-consistent field theories. *The Journal of chemical physics* **2009**, *130*.

# TOC Graphic

